Cell-Permeable Gomesin Peptide Promotes Cell Death by Intracellular Ca2+ Overload

ARTICLE *in* MOLECULAR PHARMACEUTICS · AUGUST 2012

Impact Factor: 4.38 · DOI: 10.1021/mp300251j · Source: PubMed

molecular pharmaceutics

Article

pubs.acs.org/molecularpharmaceutics

Cell-Permeable Gomesin Peptide Promotes Cell Death by Intracellular Ca^{2+} Overload

Edgar J. Paredes-Gamero,[†,‡,§] Rafael L. Casaes-Rodrigues,[†,§] Gioconda E. D. D. Moura,[†] Tatiana M. Domingues,[‡] Marcus V. Buri,[‡] Victor H. C. Ferreira,[∥] Edvaldo S. Trindade,[∥] Ana J. Moreno-Ortega,[⊥] María F. Cano-Abad,[⊥] Helena B. Nader,[†] Alice T. Ferreira,[‡] Antonio Miranda,[‡] Giselle Z. Justo,*[,†,#] and Ivarne L. S. Tersariol*[,†,¶]

[†]Departamento de Bioquímica and [‡]Departamento de Biofísica, Universidade Federal de São Paulo, Três de Maio 100, 04044-020, São Paulo, Brazil

[∥]Departamento de Biologia Celular, Universidade Federal do Paraná, PO Box 19031, 81531-990, Curitiba, Brazil

[⊥]Instituto Teófilo Hernando, Servicio de Farmacología Clínica, Instituto de Investigación Sanitaria, Hospital Universitario de la Princesa, Universidad Autónoma de Madrid, Madrid, Spain

[#]Departamento de Ciências Biológicas, Universidade Federal de São Paulo, Diadema, SP, Brazil

[¶]Centro Interdisciplinar de Investigação Bioquímica, Universidade de Mogi das Cruzes, Mogi das Cruzes, SP, Brazil

S *Supporting Information*

ABSTRACT: In recent years, the antitumoral activity of antimicrobial peptides (AMPs) has been the goal of many research studies. Among AMPs, gomesin (Gm) displays antitumor activity by unknown mechanisms. Herein, we studied the cytotoxicity of Gm in the Chinese hamster ovary (CHO) cell line. Furthermore, we investigated the temporal ordering of organelle changes and the dynamics of Ca^{2+} signaling during Gm-induced cell death. The results indicated that Gm binds to the plasma membrane and rapidly translocates into the cytoplasm. Moreover, 20 μM Gm increases the cytosolic Ca^{2+} and induces membrane permeabilization after 30 min of treatment. Direct Ca^{2+} measurements in CHO cells transfected with the genetically encoded D1-cameleon to the endoplasmic reticulum (ER) revealed that Gm induces ER Ca^{2+} depletion, which in turn resulted in oscillatory mitochondrial Ca^{2+} signal, as measured in cells expressing the genetically encoded probe to the mitochondrial matrix $_{mit}$Pericam. This leads to mitochondria disruption, loss of mitochondrial membrane potential and increased reactive oxygen species prior to membrane permeabilization. Gm-induced membrane permeabilization by a Ca^{2+}-dependent pathway involving Gm translocation into the cell, ER Ca^{2+} depletion and disruption, mitochondrial Ca^{2+} overload and oxidative stress.

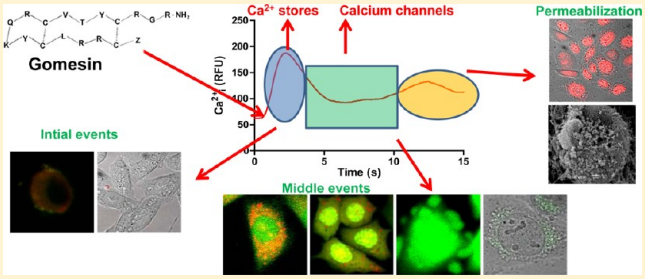

KEYWORDS: *antimicrobial peptide, gomesin, membrane permeabilization, calcium, endoplasmic reticulum, mitochondria*

INTRODUCTION

Antimicrobial peptides (AMPs) are molecules related to the immune system of nearly all organisms. Most AMPs are cationic and usually amphiphilic. They exhibit diverse structures and demonstrate cytotoxic action against microorganisms such as bacteria, fungi and other pathogenic agents. Only a few AMPs have shown potential activity as anticancer agents such as gomesin (Gm).[1−4] Gm is an AMP isolated from hemocytes of the Brazilian spider *Acanthoscurria gomesiana* containing 18 amino acid residues, including 4 cysteines engaged in two internal disulfide bridges, Cys^{2-15} and Cys^{6-11}. It contains two posttranslational modifications, a pyroglutamic acid (Z) as the N-terminus and an amidated arginine residue as the C-terminus. The entire sequence is ZCRRLCYKQRCVTYCRGR-NH_2.

Gm exhibits high cytotoxicity against bacteria, fungi, yeast, and parasites.[5−10] It is commonly assumed that the main antimicrobial mechanism of Gm and other AMPs involves membrane permeabilization. The cytolytic action of AMPs was thought to occur via a nonspecific interaction with their positive charge or amphiphilic nature, which may facilitate their insertion into lipid bilayers. This insertion leads to the subsequent formation of pores and/or the disruption of membranes of the microorganisms.[11−14] Additionally, it has been demonstrated that AMPs induce necrosis, apoptosis and autophagy in mammalian cells and tumor cell lines.[1,4,15,16] Despite the ability of Gm and other AMPs to induce cancer cell death, the details of the mechanisms related to its antitumor activity are poorly

Received: May 3, 2012
Revised: July 31, 2012
Accepted: August 7, 2012
Published: August 7, 2012

understood. In this study, we provide new insights into the molecular mechanisms involved in Gm-induced cytotoxicity in CHO cells.

EXPERIMENTAL SECTION

Peptide Synthesis. Peptides were synthesized by the solid-phase method on a 4-methylbenzhydrylamine resin (MBHAR) (0.8 mmol/g) according to the *t*-Boc strategy.[11] Full deprotection and cleavage of the peptide from the resin were carried out using anhydrous HF treatment with anisole and dimethyl sulfide (DMS) as scavengers at 0 °C for 1.5 h. The formation of disulfide bridges was achieved immediately after HF cleavage and extraction of the crude peptide. The resulting peptide solution was maintained at pH 6.8−7.0 at 5 °C for 72 h. Cyclization reactions were monitored by reversed-phase liquid chromatography coupled with an electrospray ionization mass spectrometer (LC/ESI-MS). Lyophilized crude peptides were purified by preparative RP-HPLC on a Jupiter C_{18} column (21.20 × 250 mm, 300 Å pore size, 15 μm particle size) in two steps. The first step used triethylammonium phosphate (TEAP) pH 2.25 as solvent A and 60% acetonitrile (ACN) in A as solvent B. The second step used 0.1% trifluoroacetic acid (TFA)/H_2O as solvent A and 60% ACN in A as solvent B. Pure peptides were characterized by amino acid analysis and LC/ESI-MS. Peptides were fluorescently labeled by the addition of rhodamine (rhod) to the Lys side chain by incubating 5 mg of the purified peptides, 2 mg of 5(6)-carboxytetramethylrhodamine *N*-succinimidyl ester, and 4 μL of *N*,*N*-diisopropylethylamine (DIPEA) in 500 μL of *N*,*N*-dimethylformamide (DMF) for 2 h at room temperature.[14] Gm was biotinylated (Gm−biot) by a similar experimental protocol. Briefly, biotin was coupled to the Lys side chain by incubating 8 mg of pure Gm, 2 mg of *N*-hydroxy-succinimidyl-biotin, and 6 μL of DIPEA in 500 μL of DMF for 2 h at room temperature. The resulting labeled peptides were repurified by preparative RP-HPLC using 0.1% TFA/H_2O as solvent A and 60% ACN in A as solvent B. Pure peptides were also characterized by LC/ESI-MS.

Cell Lines and Culture Conditions. Wild-type CHO-K1 cells were kindly donated by Prof. Jeffrey D. Esko (Glycobiology Research and Training Center, University of California, San Diego, La Jolla, CA, USA). CHO cells were chosen because they are widely used in transfection experiments. Cells were cultured in F-12 medium (Sigma Chemical Co., USA) supplemented with 10% fetal bovine serum (FBS; Gibco, USA), 10 U/mL penicillin and 10 μg/mL streptomycin (Sigma Chemical Co). Cells were cultured in a humidified incubator containing 2.5% CO_2 at 37 °C.

Cell Viability Assay. CHO cells were incubated in 96-well microtiter plates in F-12 medium supplemented with 10% FBS until reach the semiconfluence, and then treated with different concentrations of Gm for 24 h. To investigate the mechanisms of Gm-induced cell death, CHO cells were also pretreated with necrostatin-1 (10 μM) or Z-VAD (20 μM) for 2 h. Cell viability was determined using the standard reduction of the tetrazolium salt 3-(4,5-dimethylthiazol-2-yl)-2,5-diphenyltetrazolium bromide (MTT). The results were expressed relative to control cell viability (100%).

Calcein Release Assay. CHO cells (2×10^4 cells/well) were cultured for 24 h in black 96-well microplates and then incubated with 1 μM calcein-AM (Invitrogen, USA) for 40 min. Cells were subsequently washed twice with HBSS and treated with 10 or 20 μM Gm. Calcein fluorescence was quantified in a FlexStation 3 microplate reader with excitation at 490 nm and emission at 525 nm. Maximum release of calcein (100%) was determined by the addition of 0.001% Triton X-100.

Cell Death by the Annexin V and 7-AAD Assay. Cells were treated with 10 or 20 μM Gm for 4 h and subsequently harvested, washed with PBS and resuspended in binding buffer (0.01 M HEPES, pH 7.4, 0.14 M NaCl and 2.5 mM $CaCl_2$) at a concentration of 5×10^5 cells/mL. The suspensions were labeled with annexin (An) V-APC and 5 μg/mL 7-amino-actinomycin D (7-AAD) (BD Biosciences, USA) according to the manufacturer's instructions. After incubation at room temperature for 20 min, cells were analyzed in a FACSCalibur flow cytometer (Becton Dickinson, USA) using CellQuest software (Becton Dickinson, USA). A total of 10,000 events were collected per sample.

Cellular Evaluation by Confocal Microscopy. The in vivo incorporation of Gm−rhod was evaluated by confocal microscopy. All images were captured and processed using a LSM 510 META confocal microscope (Zeiss, Germany) with a 63× objective (Plan-Neofluar, 1.4 numerical aperture) under oil immersion. The Gm−rhod was excited with a HeNe laser (λ_{Ex} = 543 nm), and light emission was detected using a Zeiss META detector (λ_{Em} = 560−600 nm). Images were collected approximately every 15 s. Fluorescence intensity was normalized to the basal fluorescence using Examiner 3.2 (Zeiss, Germany) and Spectralyzer (USA) software.[17]

CHO cells were also stained with different fluorophores in F-12 medium for 30 min at 37 °C and then washed with Hanks balanced salt solution (HBSS: 137 mM NaCl, 5.4 mM KCl, 0.25 mM Na_2HPO_4, 0.44 mM KH_2PO_4, 1.3 mM $CaCl_2$, 1.0 mM $MgSO_4$ and 4.2 mM $NaHCO_3$). Mitochondria were labeled with 100 nM MitoTracker Green (Invitrogen, USA), and the mitochondrial transmembrane potential ($\Delta\Psi_{mit}$) was measured using 100 nM tetramethylrhodamine ethyl ester (TMRE; Invitrogen, USA). ER was labeled using ER-Tracker Blue-White DPX (Invitrogen, USA). For the lysosomal leakage assays, cells were labeled with 5 μg/mL acridine orange (AO; Sigma Chemical Co., USA). Additionally, 1 μM LysoTracker Green (Invitrogen, USA) was used to label the lysosomes. To measure reactive oxygen species (ROS), CHO cells were incubated with 10 μM DCFDA. Cellular membrane permeabilization was monitored by the incorporation of 1 μM Sytox Green (Invitrogen, USA) or 5 μg/mL propidium iodide (PI) (Sigma) into the nucleus. Images were collected at approximately 10−30 s intervals.

To monitor trafficking to the early endosomes, CHO cells were transfected with CellLight Early Endosomes-GFP Bacman 2.0 (Invitrogen, USA). Early endosome distribution was viewed by confocal microscopy of live cells. Briefly, 10^4 CHO cells/well were incubated overnight and transfections were then performed according to the manufacturer's instructions.

Sytox Green, DCFDA, LysoTracker Green, MitoTracker Green and Early Endosomes-GFP were excited using an argon laser (λ_{Ex} = 488 nm), and their emissions were detected using a META detector (λ_{Em} = 500−550 nm). TMRE was excited with a HeNe laser (λ_{Ex} = 543 nm), and the emission was detected using a Zeiss META detector (λ_{Em} = 560−610 nm). AO was excited using an argon laser (λ_{Ex} = 488 nm), and the green fluorescence (λ_{Em} = 500−560 nm) and red fluorescence (λ_{Em} = 600−700 nm) were captured using a META detector. PI was excited with an argon laser (λ_{Ex} = 488 nm), and the emission was detected using a Zeiss META detector (λ_{Em} = 580−650 nm). R-Tracker Blue-White DPX was excited with a multiphoton laser

(λ_{Ex} = 750 nm), and the emission was detected using a Zeiss META detector (λ_{Em} = 530−590 nm)

Ca^{2+} Measurement. To measure the cytoplasmic and mitochondrial Ca^{2+} concentrations ($[Ca^{2+}]_c$ and $[Ca^{2+}]_{mit}$, respectively), CHO cells were incubated with 4 μM Fluo-4/AM and 5 μM Rhod-2/AM, respectively, for 30 min at 37 °C. Fluo-4 was excited with an argon laser (λ_{Ex} = 488 nm), and the light emission was detected using a Zeiss META detector (λ_{Em} = 500−550 nm). Rhod-2 was excited with a HeNe laser (λ_{Ex} = 543 nm), and the emission was detected using a META detector (λ_{Em} = 560−620 nm).[17,18] The pinhole device was not used. Images were collected at approximately 10 s intervals. Fluorescence intensity was normalized as previously described.[17,18]

$[Ca^{2+}]_c$ measurements were also determined by incubating 2×10^4 CHO cells/well in black 96-well microplates with the Fluo-4 Direct Calcium Assay reagent according to the manufacturer's instructions (Invitrogen, USA). After 1 h of indicator incorporation at 37 °C, cells were stimulated and the fluorescence was quantified in a FlexStation 3 microplate reader (Molecular Devices, USA). The Fluo-4 was excited at 490 nm, and the emission was detected at 525 nm.[19]

Additionally, $[Ca^{2+}]_{ER}$ and $[Ca^{2+}]_{mit}$ changes were measured by transfection of CHO cells with ER-targeted D1-cameleon and $_{mit}$Pericam, respectively. Transfection of CHO cells was achieved using the jetPEI transfection reagent (Polyplus-transfection, USA) according to the manufacturer's instructions. A total of 4×10^4 cells were incubated for 24 h in 12 mm diameter coverslips, and then transfected with jetPEI solution containing 1 μg of cDNA encoding either D1-cameleon or $_{mit}$Pericam (a gift from Dr. Roger Tsien). After 48 h in culture, the coverslips were set in the stage of an upright fluorescence microscope (BX51WI, Olympus) with an Olympus 40× objective (1.0 numerical aperture). For ratiometric D1-Cameleon measurements, an excitation wavelength of 440 nm and emission wavelengths of 512 and 480 nm were used. $_{mit}$Pericam excitation was alternatively performed at 410 and 480 nm, and the emission was collected at 512 nm. Images were captured using a CCD camera (Sony, Japan). Synchronization of the filter wheel and the CCD camera and raw data acquisition were performed with the Olympus Cell R software (version 2.6). The ratio of D1-cameleon (512/480) and $_{mit}$Pericam (480/410) fluorescence was calculated using the Image J software.

Scanning Electron Microscopy. The cells were fixed with 2.5% glutaraldehyde in 0.1 M cacodylate buffer, pH 7.2, washed and postfixed in 1% OsO_4 for 30 min in the dark at room temperature. After washing, cells were dehydrated in increasing ethanol concentrations. Cells were CO_2 critical point dehydrated, metalized and observed in a JEOL JSM-6360 LV scanning electron microscopy for alterations in the cell membrane.

ATP Content. The cellular ATP content was determined after 4 h of treatment using the ATP assay mix (luciferase, luciferin, $MgSO_4$, DTT, EDTA, BSA, and tricine buffer salts), which is based on the bioluminescent measurement of ATP after cell lysis according to the manufacturer's instructions (Sigma-Aldrich). The luminescence intensity was measured in a FlexStation 3 microplate reader.

Statistical Analysis. The fluorescence intensity was normalized to basal intensity (F_t/F_0) and is shown as a representative pseudocolored image according to a fluorescence intensity scale ranging from 0 (black) to 255 (white) or using a ratio of D1-cameleon and $_{mit}$Pericam. All data represent at least three independent experiments and are expressed as the mean ± standard error of the mean (SEM). Statistical analyses were performed using Student t test for comparison between two groups and analysis of variance (ANOVA) and Dunnett's post hoc test for multiple comparisons among groups. A probability (P) value greater than 0.05 was considered significant.

RESULTS

Gomesin Induces CHO Cell Death by Membrane Permeabilization. In order to establish the cytotoxic effect of Gm in CHO cells, a concentration−response curve was performed. The assessment of cytotoxicity by the MTT assay demonstrated that Gm promotes cell death with an IC_{50} of 10 μM (Figure 1A). Gm cytotoxic mechanism was investigated using An-V and 7-AAD staining. CHO cells stimulated with 10 and 20 μM Gm for 2 h showed major double-positive staining (Figure 1B). Similar results were obtained after 24 h of treatment (Supporting Information, Figure S1A). DIC time-lapse images in the presence of the nuclear stain PI, a membrane-impermeant fluorophore, indicated rapid PI incorporation into the nucleus and alterations in the plasma membrane after treatment with Gm (Figure 1C and video 1 in the Supporting Information). The loss of cell membrane integrity was further investigated using calcein, which reveals that 20 μM Gm induced around 10% and 50% of membrane permeabilization after 7 and 20 min of treatment, respectively (Figure 1D). However, low cell permeabilization was induced after 40 min of treatment with 10 μM Gm (Figure 1D). Alterations in plasma membrane and cell shape were also seen after labeling CHO cells with wheat germ agglutinin (Supporting Information, Figure S1B). Direct evidence of the effect of 20 μM Gm on cell membrane permeabilization was obtained by scanning electron microscopy (Figure 1E and Supporting Information, Figure S1C). In addition, morphological alterations in organelles such as mitochondria ($_{mit}$Pericam) and ER (D1-cameleon) were observed in transfected cells with specifically decoding proteins (Supporting Information, Figure S1D).

Gm Induces an Increase in Cytosolic Ca^{2+}. Calcium is a universal second messenger with a pivotal role in cell death.

The involvement of Ca^{2+} on Gm-induced necrosis was evaluated by loading CHO cells with the Ca^{2+} probe Fluo-4. Changes in cytosolic Ca^{2+} concentration ($[Ca^{2+}]_c$) were analyzed after treatment with 20 μM Gm. Figure 2A shows that Gm induced a biphasic $[Ca^{2+}]_c$ response characterized by two components, an initial transient increase of $\Delta 147 \pm 10$ RFU (relative fluorescence units) (initial phase) followed by a sustained plateau $\Delta 65 \pm 14$ RFU (sustained phase). As Gm induces membrane permeabilization, a comparison between the fluorescence maximum elicited by Gm and A23122, a Ca^{2+} ionophore, is shown in Figure 2A as an inset. Additionally, the Gm-induced initial increase in $[Ca^{2+}]_c$ did not decrease in nominally Ca^{2+}-free solution ($0Ca^{2+}$) or in $0Ca^{2+}$ solution containing EGTA, an extracellular Ca^{2+} chelator (Figure 2B,C). In contrast, the sustained response was abolished in $0Ca^{2+}$ solution with or without EGTA (Figure 2B,D). The complete emptying of the ER by treatment with 500 μM caffeine, 10 μM ryanodine and 1 μM thapsigargin (CRT) abolished the Ca^{2+} increase induced by 20 μM Gm (Figure 2E). Thus, the initial phase occurs as a consequence of the release of Ca^{2+} from the intracellular stores, and the sustained phase is dependent on the extracellular Ca^{2+}. Moreover, BAPTA, an intracellular Ca^{2+} chelator, was able to inhibit Gm-induced cell death (Figure 2F), while Z-VAD, a pan-caspase inhibitor, and necrostatin-1, a receptor-interacting protein 1 kinase inhibitor, did not affect cell viability (Supporting Information, Figure S2A).

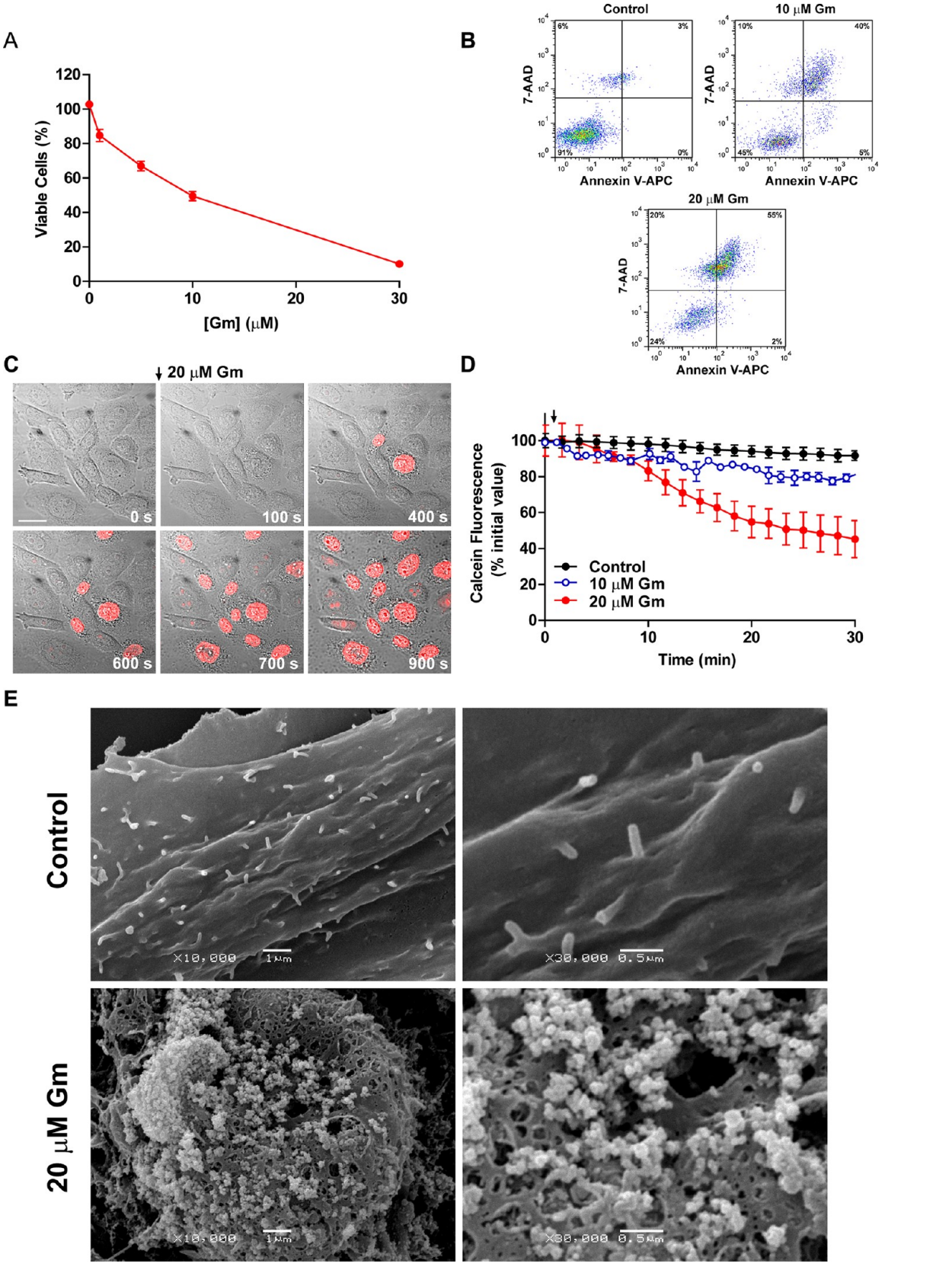

Figure 1. Gm promotes cell death by membrane permeabilization. The cytotoxic activity of Gm was assessed by the MTT reduction test and the An-V/7-AAD staining (panels A and B, respectively). (A) Concentration-dependent effect of Gm in CHO cells after 24 h of treatment. (B) Analysis of An-V/7-AAD staining after treatment of cells with 10 and 20 μM Gm for 2 h. (C) Cells were treated with 20 μM Gm in the presence of 5 μg/mL PI. Time-lapse images of PI internalization were captured by confocal microscopy. (D) Cells were incubated with 1 μM calcein for 40 min and then treated with 20 μM Gm. Calcein fluorescence was quantified in a Flex Station 3 microplate reader. (E) Scanning electron microscopy after treatment with 20 μM Gm for 24 h (10000× and 30000× magnification). (A and D) The data are expressed as the mean ± SEM of four independent experiments run in triplicate. *$p < 0.05$; ANOVA, Dunnett's post hoc test.

dx.doi.org/10.1021/mp300251j | *Mol. Pharmaceutics* 2012, 9, 2686−2697

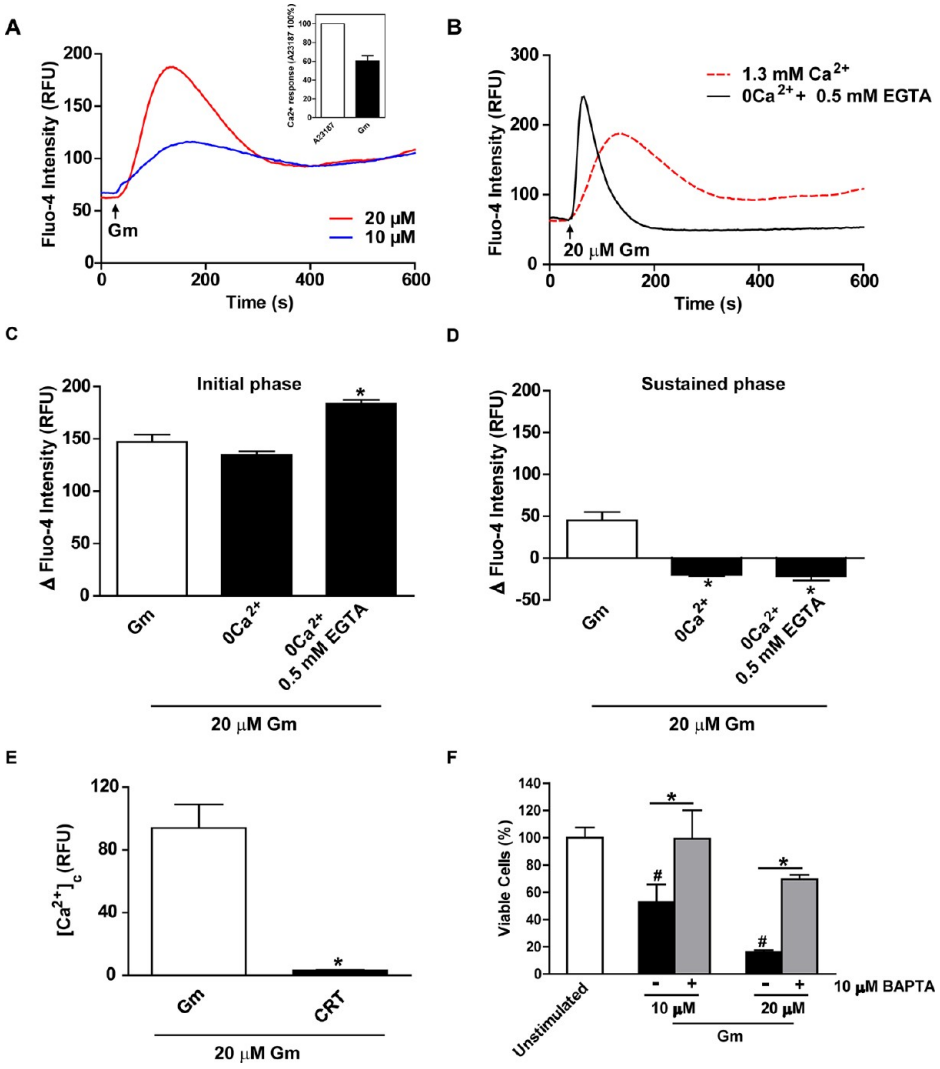

Figure 2. Characterization of the Gm-induced Ca^{2+} response. Changes in $[Ca^{2+}]_c$ levels measured as relative fluorescence units (RFU) in Fluo-4 loaded CHO cells. (A) Gm at 10 and 20 μM induced a concentration-dependent increase in $[Ca^{2+}]_c$. Two components of $[Ca^{2+}]_c$ response can be observed, an initial response followed by a sustained response. (B) Lack of a sustained response in cells treated with 20 μM Gm in $0Ca^{2+}$/EGTA solution. (C) Quantification of the initial phase and (D) the sustained Ca^{2+} response expressed as RFU intensity. (E) Emptying the ER with 1 mM caffeine, 10 μM ryanodine and 1 μM thapsigargin (CTR) abolished the $[Ca^{2+}]_c$ increase promoted by Gm. (F) Prior incubation with BAPTA for 1 h inhibits Gm-promoted cell death. Viability was assessed using the MTT test. (A and B) Typical results of at least three independent experiments are shown. (C and F) The data are expressed as the mean ± SEM of three independent experiments performed in triplicate. *$p < 0.05$; ANOVA, Dunnett's post hoc test or Student t test.

Gm Induces Ca^{2+} Release from the Endoplasmic Reticulum. Due to the results showing that the sustained phase was dependent on extracellular Ca^{2+}, the participation of store-operated Ca^{2+} channels (SOCC) in Gm effect was verified using a classical protocol of SOCC opening.[20] As a control of SOCC opening, CHO cells were stimulated with 1 μM thapsigargin (Thap) in a $0Ca^{2+}$ solution, and then Ca^{2+} was added (Figure 3A). The same protocol was used to verify the effect of 20 μM Gm, and similarly to Thap, the release of intracellular Ca^{2+} stores induced by Gm stimulated SOCC opening (Figure 3B).

In addition, we evaluated the effect of the enantiomer D-Gm. As the native molecule, D-Gm acts by inducing $[Ca^{2+}]_c$ increase and cell death (Supporting Information, Figure S3A,B).

To direct measure the bulk increase in $[Ca^{2+}]_c$ induced by Gm, CHO cells were transfected with the ER-targeting Ca^{2+} probe D1-cameleon, which is specific for ER $[Ca^{2+}]$ measurements ($[Ca^{2+}]_{ER}$). The results indicated that 20 μM Gm induces the release of $[Ca^{2+}]_{ER}$ with similar efficacy in the presence of 1.3 mM Ca^{2+} (Figure 3C) and in $0Ca^{2+}$/EGTA solution (Figure 3D). The quantification of $[Ca^{2+}]_{ER}$ release is shown in Figure 3E. To verify the integrity of the ER in CHO cells after Gm treatment, ATP, a P2 receptor agonist that induces the release of Ca^{2+} from intracellular stores, was used.[21] After treatment with a low concentration of Gm (5 μM), ATP was unable to induce the release of the same amount of Ca^{2+} from the ER (Supporting Information, Figure S4A). Moreover, rapid morphological changes in the ER were observed after treatment with 20 μM Gm (Figure 3F). Figure 3G shows confocal images performed using 1 μM Gm conjugated to rhodamine (Gm−rhod), in order to avoid the permeabilization, and ER-Tracker leak. The images are a focal plane Z. This figure shows partial colocalization (30%) of Gm in ER (Figure 3G).

Gm Promotes Mitochondrial Ca^{2+} Overload and Dysfunction before Membrane Permeabilization. Mitochondria

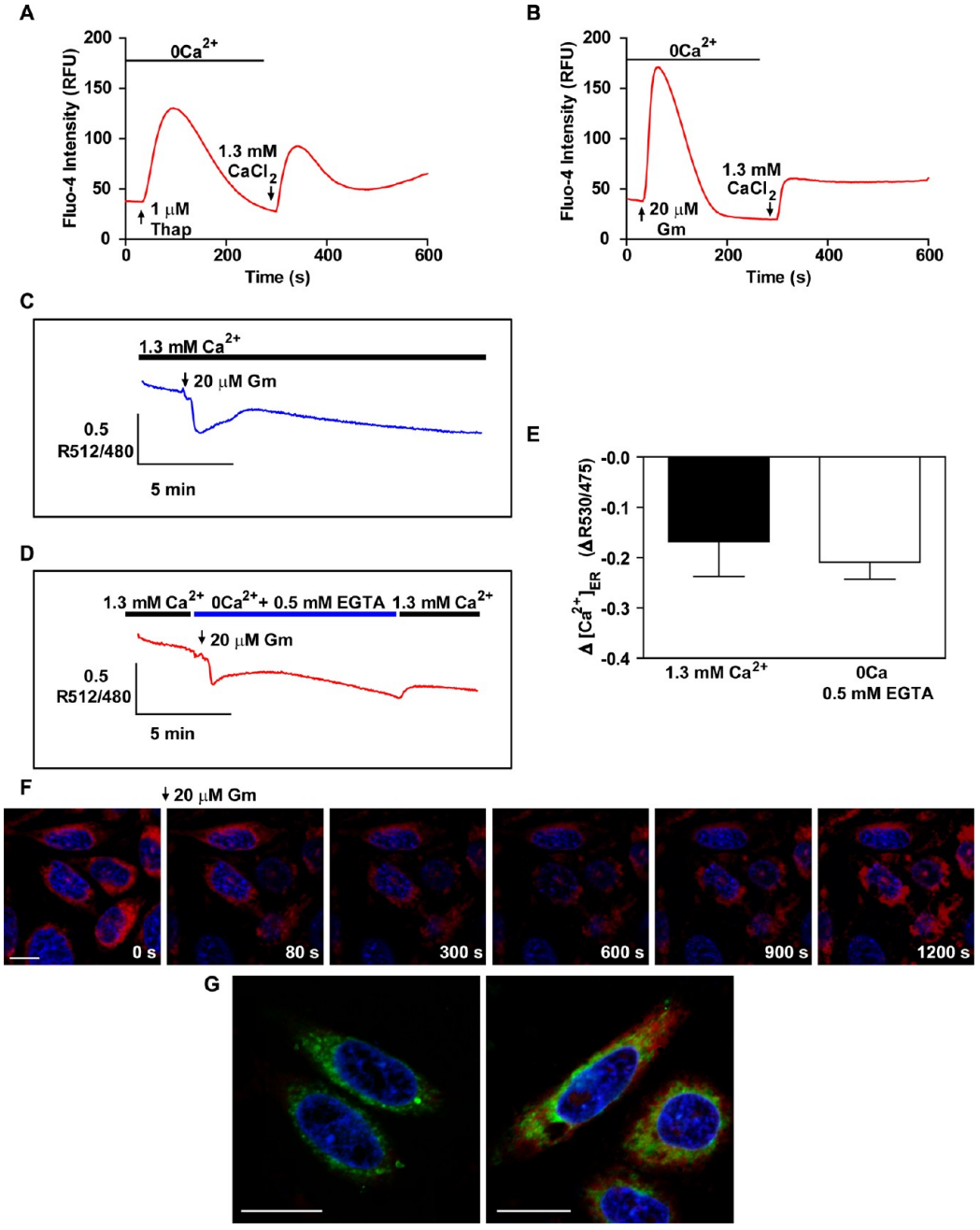

Figure 3. Gm released Ca^{2+} from the ER and induced SOCC opening. (A) CHO cells were loaded with the Ca^{2+} probe Fluo-4. (A) Cells were treated with 1 mM Thap or (B) 20 μM Gm in $0Ca^{2+}$ solution, and then the reintroduction of 1.3 mM Ca^{2+} resulted in SOCC opening and $[Ca^{2+}]_c$ increased. Typical results of three independent experiments are shown. Changes in the $[Ca^{2+}]_{ER}$ induced by 20 μM Gm were estimated in CHO cells transiently expressing the Ca^{2+} probe directed to the ER, D1-cameleon, in (C) 1.3 mM Ca^{2+} solution or in (D) a $0Ca^{2+}$/EGTA solution. (E) Quantification of $[Ca^{2+}]_{ER}$ after treatment with 20 μM Gm in 1.3 mM Ca^{2+} or in $0Ca^{2+}$/EGTA solution. (F) CHO cells stained with ER-Tracker red and treated with 20 μM Gm promoted ER disruption. Time-lapse images were captured by confocal microscopy. The data are expressed as the mean ± SEM. 8−10 cells were evaluated by group in 4 independent experiments. (G) The cells were loaded with ER-Tracker Blue/White (green) for 20 min, and then they were stimulated with 1 μM Gm−rhod (red) for 5 min. Nuclei were labeled with DAPI (blue). Confocal images were performed in one focal plane. Secondary control is shown on the left. Image of cells stimulated with Gm−rhod is shown on the right.

are protagonists of cell death and potential targets of AMPs.[22] Thus, alterations in mitochondrial transmembrane potential (Ψ_{mit}) and morphology induced by Gm were monitored. Cell staining with MitoTracker Green showed mitochondrial disruption after 20 μM Gm treatment (Figure 4A). The Ψ_{mit} was measured with TMRE in the presence of SYTOX Green, a membrane-impermeant fluorophore. Temporal microscopy evaluation revealed that the loss of $\Delta\Psi_{mit}$ occurred prior to membrane permeabilization (Figure 4B,C and video 2 in the Supporting Information), although, not all cells exhibited signs of membrane permeabilization after the decrease in Ψ_{mit}.

Single cell analysis of Fluo-4 and Rhod-2 fluorescence revealed that 20 μM Gm induced oscillatory $[Ca^{2+}]_c$ and $[Ca^{2+}]_{mit}$ increases until membrane disruption occurred (Figure 4D). Moreover, temporal quantification of the Ca^{2+} signal showed a transient increase in $[Ca^{2+}]_c/[Ca^{2+}]_{mit}$ (Figure 4E) that was

dx.doi.org/10.1021/mp300251j | Mol. Pharmaceutics 2012, 9, 2686−2697

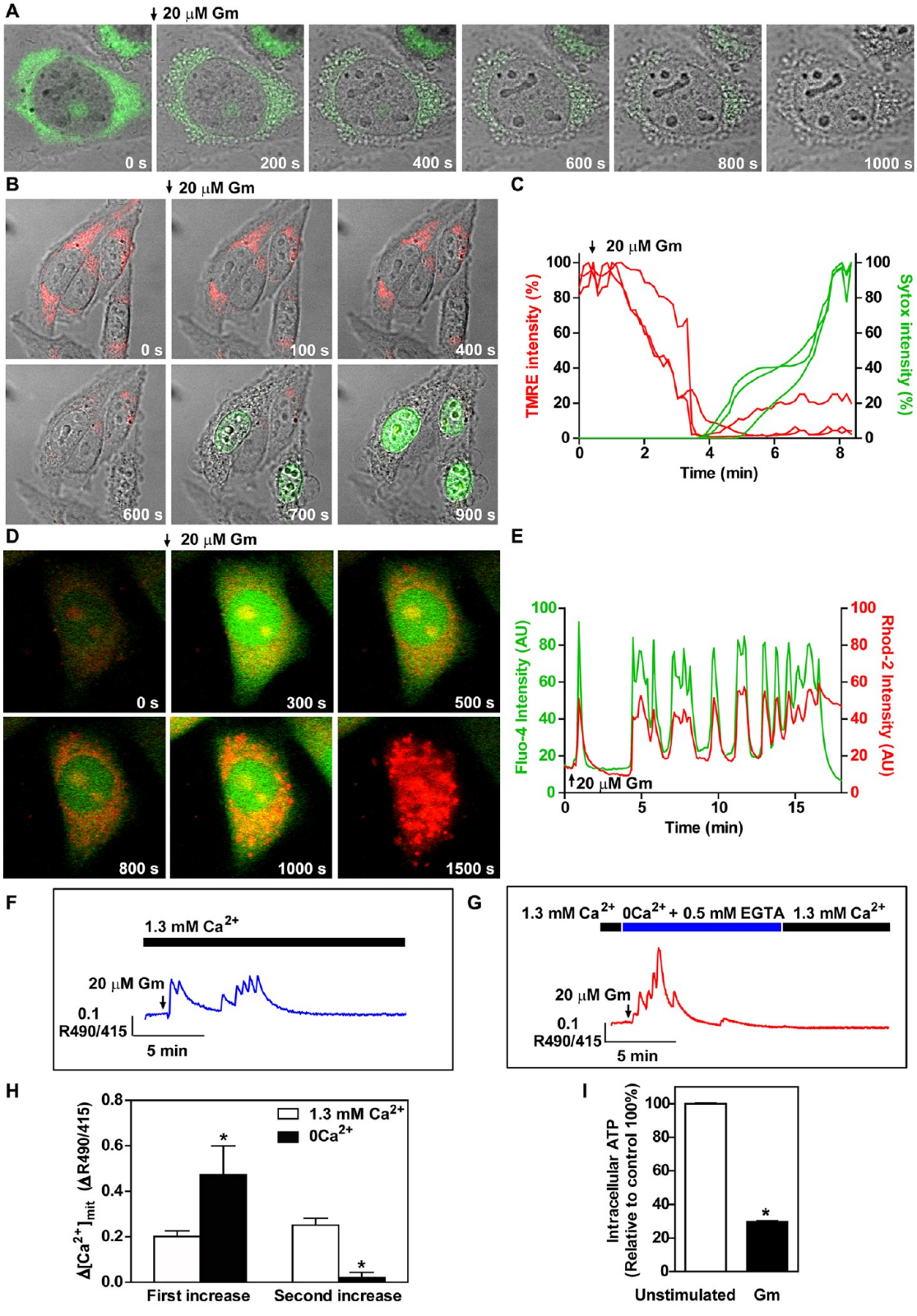

Figure 4. Mitochondrial uptake of Ca^{2+} elicited by Gm. (A) Time-lapse images using DIC with MitoTracker Green to stain the mitochondria. (B, C) The Ψ_{mit} (red) was measured by loading the cells with TMRE in the presence of SYTOX Green (green). (B) Time-lapse images of Ψ_{mit} and SYTOX fluorescence. (C) Quantification of TMRE and SYTOX Green fluorescence from the images shown in B. Each trace represents an individual cell. (D, E) $[Ca^{2+}]_c$ and $[Ca^{2+}]_{mit}$ were quantified in CHO cells incubated with Fluo-4 (green) and Rhod-2 (red), respectively. (D) Confocal time-lapse images of $[Ca^{2+}]_c$ and $[Ca^{2+}]_{mit}$. (E) Quantification of Fluo-4 and Rhod-2 fluorescence shown in D. (F–H) CHO cells were transfected with $_{mit}$Pericam, and changes in $[Ca^{2+}]_{mit}$ were estimated on the basis of 490/415 fluorescence ratio. Typical response of $[Ca^{2+}]_{mit}$ after treatment with 20 μM Gm in (F) normal Ca^{2+} conditions and in (G) a $0Ca^{2+}$ containing EGTA solution. (H) Quantification of $[Ca^{2+}]_{mit}$. (I) ATP content measurements were performed by an ATP bioluminescent assay. (H–I) The data are expressed as the mean ± SEM. (H) 12–18 cells were evaluated by group in 6 independent experiments. (I) The experiment was performed in triplicate. *$p < 0.05$; Student t test.

dx.doi.org/10.1021/mp300251j | *Mol. Pharmaceutics* 2012, 9, 2686–2697

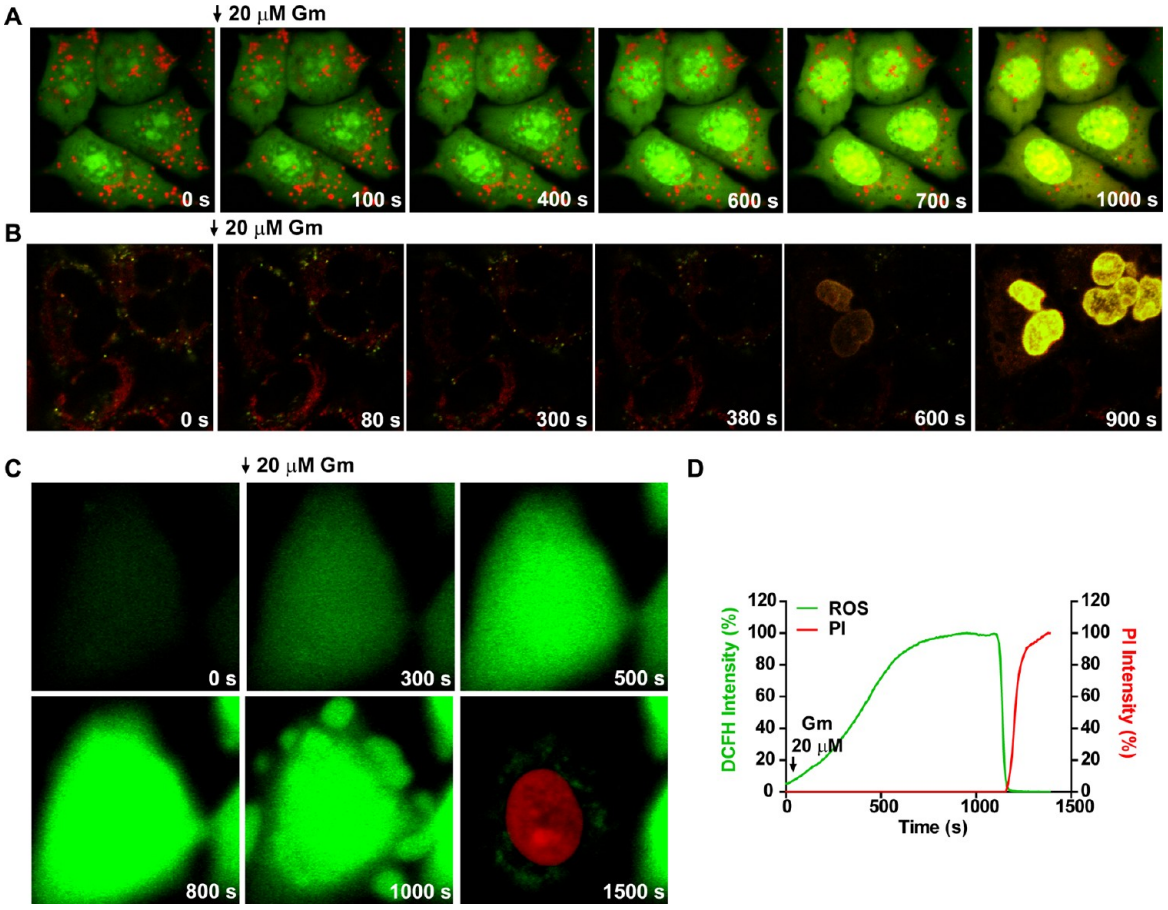

Figure 5. Gm promoted endosomal/lysosomal disruption and ROS increase. (A) The lysosomal/endosomal leakage induced by 20 μM Gm was monitored after labeling cells with 5 μg/mL of the vital dye AO for 15 min. (B) The acidic vesicles of the endocytic compartments of CHO cells were labeled with 1 μM LysoTracker Green (green) and 100 nM TMRE (red) for 30 min. Time-lapse images were collected by confocal microscopy in the presence of SYTOX Green (nucleus). (C, D) ROS were quantified by the synthetic probe DCFH-DA. (C) Time-lapse images of DCFH (green) were collected in the presence of PI (red). (D) Quantification of DCFH and PI fluorescence in panel C.

followed by an oscillatory $[Ca^{2+}]_c/[Ca^{2+}]_{mit}$ signal (Figure 4D,E and video 3 in the Supporting Information). To directly address the question of whether the $[Ca^{2+}]$ released from the ER was uptaken by mitochondria, experiments were performed in cells transfected with genetically encoded Ca^{2+} sensors.[23,24] An elevation in the $[Ca^{2+}]_{mit}$ with an oscillatory pattern was observed after treatment of CHO cells transiently expressing $_{mit}$Pericam with 20 μM Gm (Figure 4F). Interestingly, the oscillatory $[Ca^{2+}]_{mit}$ signal was abolished in a $0Ca^{2+}$/EGTA solution (Figure 4G). Quantification of $[Ca^{2+}]_{mit}$ showed that the first oscillatory events are potentiated in a $0Ca^{2+}$/EGTA solution (Figure 4H). Moreover, Gm induced a reduction in intracellular ATP levels as indicated in Figure 4I. In addition, BAPTA was able to reduce the percentage of cells with mitochondria potential decrease (Supporting Information, Figure S4B).

Gm Affects Lysosomes Integrity. Additionally, alterations in lysosome integrity were also observed using the vital fluorogenic dye acridine orange (AO). A time-dependent decrease in red fluorescence of lysosomes was observed after incubation with 20 μM Gm, indicating leakage of the AO from the lysosomes to the cytosol (Figure 5A). To determine the sequence of events, lysosomes and mitochondria were stained with LysoTracker and TMRE, respectively. Rupture of lysosomes concurrently with loss of Ψ_{mit} was observed prior to membrane permeabilization (Figure 5B). Moreover, we evaluated whether mitochondrial disruption was followed by an increase in ROS using the ROS-sensitive fluorophore DCFH-DA. As observed in Figure 5C, Gm leads to an increase in ROS prior to membrane permeabilization. The quantification of ROS increase and the entry of PI are shown in Figure 5D and video 4 in the Supporting Information. Moreover, BAPTA was able to reduce the rate of lysosome rupture (Supporting Information, Figure S4C).

Gm Is Internalized into the Cells. CHO cells transfected with a protein directed to Early Endosomes-GFP were incubated with 20 μM Gm−rhod. Temporal images revealed the entry of Gm−rhod from the edges to the center of the cell, leading to a disruption and migration of endosomes; however, colocalization was not observed with early endosomes (Figure 6A and video 5 in the Supporting Information). Additionally, the use of differential interference contrast (DIC) showed that Gm−rhod enters into the edges and is accumulated into some vesicles prior to membrane disruption (blue arrows) (Figure 6B). Quantification of the fluorescence in the cytoplasm indicated a small increase in the fluorescence, which corresponds to the translocation of Gm−rhod prior to the large increase due to membrane permeabilization (Figure 6B,C).

To further investigate the ability of Gm to interact with cell membranes, experiments were carried out at 37 °C and 4 °C. CHO cells were treated with Gm at both temperatures for 30 min, washed and cultivated for another 2 h period. Cell death was evaluated by An-V and 7-AAD staining. A significant reduction

dx.doi.org/10.1021/mp300251j | Mol. Pharmaceutics 2012, 9, 2686−2697

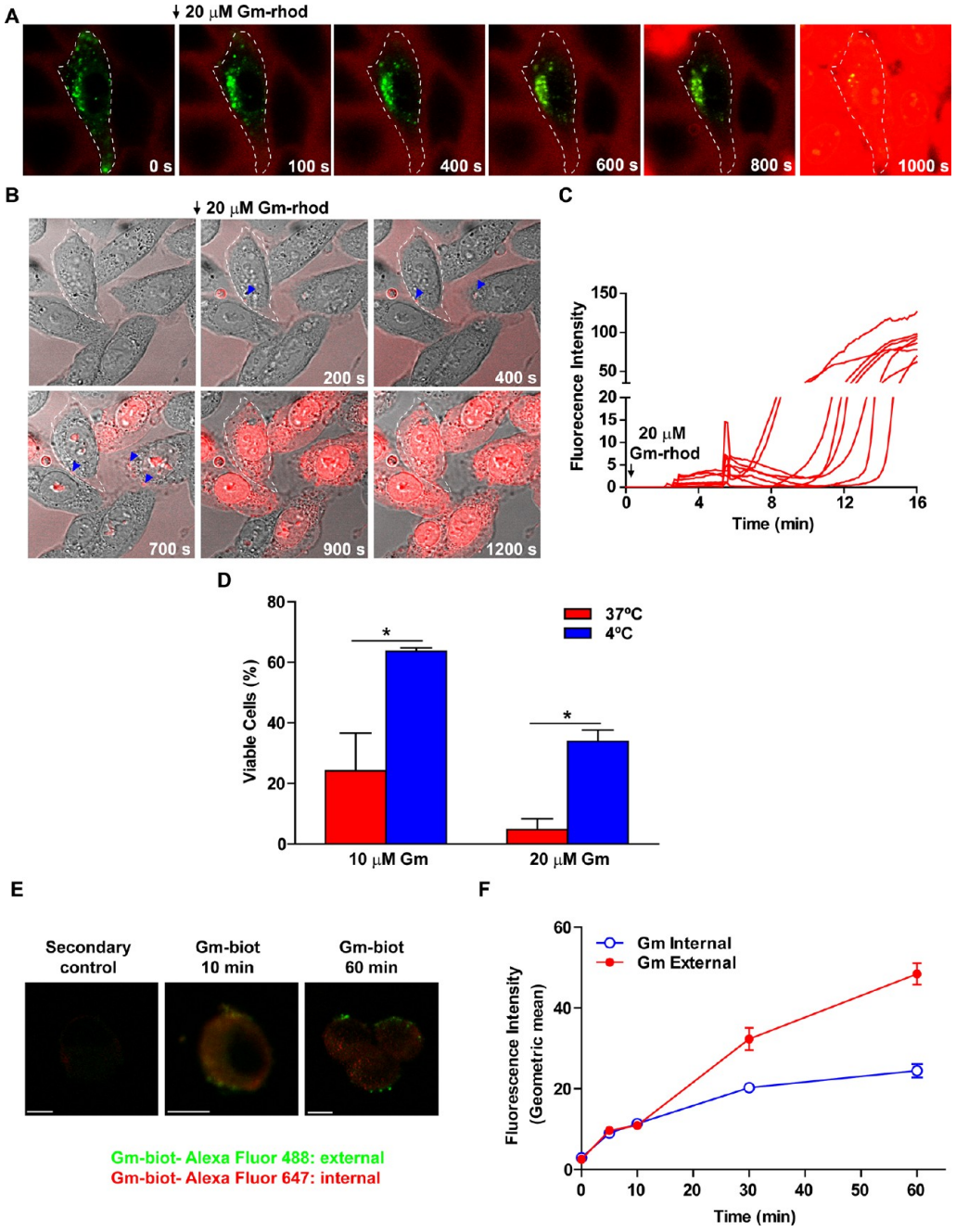

Figure 6. Rapid translocation of Gm into the cytoplasm. (A) Time-lapse images of early endosomes (green) were obtained after transfection of CHO cells with CellLight Early Endosomes-GFP Bacman 2.0. CHO cells were treated with Gm−rhod (red). White traces mark the edges of cells. (B) Cells were treated with Gm−rhod, and time-lapse images were captured by confocal microscopy using red fluorescence and DIC. Arrows indicate the vesiculation of Gm−rhod in cells. (C) Quantification of Gm−rhod fluorescence in panel B. (D) CHO cells were treated with 20 μM Gm for 1 h, washed and incubated for an additional 2 h in culture medium. Cell death was quantified by the An-V/7-AAD assay. (E and F) After treatment of cells with 1 μM Gm−biot for different times, external Gm−biot was labeled with streptavidin-Alexa Fluor 488 and internal Gm−biot was labeled with streptavidin-Alexa Fluor 647. Permeabilized cells were excluded using PI. (E) Confocal microscopy revealed Gm on the cell membrane (green) and translocated into the intracellular compartment (red). (F) Quantification of external and internal Gm−biot was performed by flow cytometry. Three independent experiments were performed in duplicate. (D and F) The data are expressed as the mean ± SEM of 3 independent experiments. *$p < 0.05$; Student t test.

in cell death was observed at 4 °C (Figure 6D). To quantify the binding of Gm to the cell membrane and its entry into cells, Gm conjugated to biotin (Gm−biot) was used at a low concentration to avoid membrane permeabilization. Dead cells were excluded using PI staining. External Gm−biot was labeled with streptavidin-Alexa Fluor 488 (green), and internal Gm−biot was labeled with streptavidin-Alexa Fluor 647 (red) as shown in Figure 6E. The temporal quantification of labeling with Gm−biot was performed by flow cytometry. A time-dependent increase in the cell membrane labeling and in the intracellular compartment was determined (Figure 6F). Moreover, the cytosolic Ca^{2+} time responses for Gm and ATP were compared and stimulation with ATP and Gm was carried out simultaneously. Logarithmic growth rates of the Ca^{2+} response for ATP and Gm were 659 and 193, respectively, demonstrating that $[Ca^{2+}]_c$ mobilization by ATP through receptors is faster than the response promoted

dx.doi.org/10.1021/mp300251j | *Mol. Pharmaceutics* 2012, 9, 2686−2697

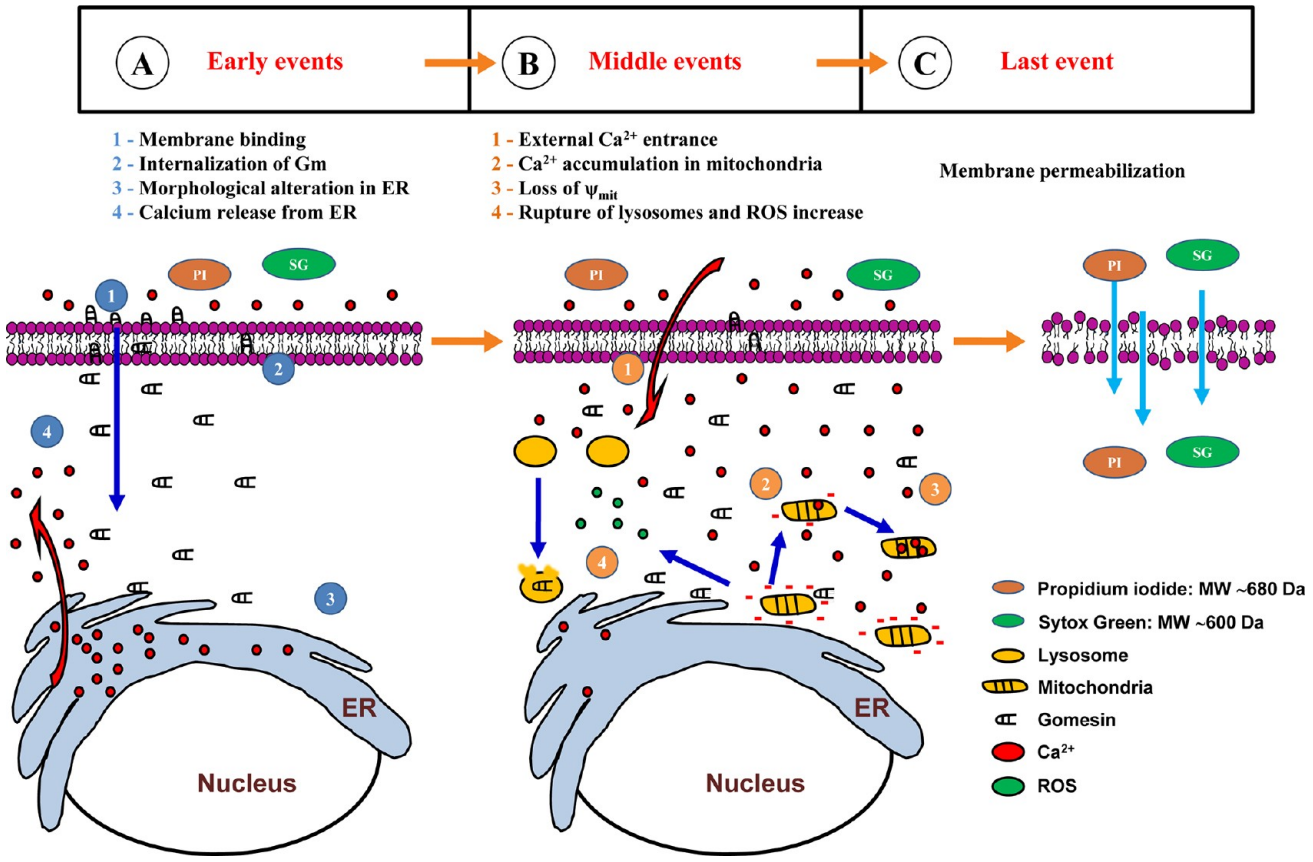

Figure 7. Proposed model of cell death induced by the Gm in CHO cells. The effects of cell death Gm-induced can be distinguished in three different moments. (A) Early events: (1) After stimulation with Gm the peptide is (2) internalized through the cell membrane, (3) promoting the morphologic alteration in the ER and (4) releasing Ca^{2+} from stores. (B) Middle events: The ER alteration also promotes (1) the entry of Ca^{2+} of extracellular medium, followed by (2) the uptake of Ca^{2+} by mitochondria, which causes (3) the loss of $\Delta\Psi_{mit}$. (4) The collapse of mitochondria accompanies the increase of free radicals and lysosome disruption. (C) Last events: The membrane permeabilization occurs.

by Gm, which possibly involves a translocation mechanism (Supporting Information, Figure S5).

DISCUSSION

It is commonly assumed that the main antimicrobial mechanism of Gm and other AMPs involves membrane permeabilization. The cytotoxic action of AMPs could occur through a non-specific interaction or an intracellular-mediated mechanism. The positive charge and the amphiphilic nature of AMPs can facilitate their insertion into lipid bilayers with the subsequent formation of pores and/or membrane disruption of the microorganisms.[11−14] The induction of melanoma cell death by Gm was previously demonstrated to occur with cell membrane permeabilization as indicated by the release of LDH.[1] Additionally, the participation of Ca^{2+} in Gm-induced cell death was recently described in human neuroblastoma SH-SY5Y and rat pheochromocytoma PC12 cells.[25] Herein, we provide deep insights into the cellular alterations in Ca^{2+} homeostasis and organelle integrity promoted by the entry of Gm into cells, which ultimately lead to membrane permeabilization and cell death.

The events promoted by Gm are initiated by the rapid translocation of Gm into the cytoplasm (Figure 6B,C). Additionally, at low temperature Gm-induced cell death is significantly inhibited (Figure 6D). Moreover, we determined that the binding of Gm to the cellular membrane and its accumulation in intracellular compartments were a time-dependent event (Figure 6F). The entry of AMPs into eukaryotic cells has been previously described,[26,27] and different translocation mechanisms were proposed depending on the AMP. In a comparative study using magainin 2, buforin 2 and a cell-penetrating peptide YGRKKRRQRRR, it was shown that the cellular uptake of magainin 2 was reduced at low temperature.[26] Moreover, this uptake was proposed to be facilitated by the transient formation of a toroidal pore, as the membranes are less fluid at low temperatures.[26] In particular, Gm demonstrates a rapid effect on Ca^{2+} release from the ER (peak around 26 s). However, its activity is slower than the P2 receptor activation (peak around 10 s) (Supporting Information, Figure S5). This observation is consistent with the time elapsed between Gm treatment and the occurrence of ER morphological changes (Figure 3D). The quantification of Gm−rhod into cells by confocal microscopy (Figure 6C) shows an early Gm entry into cells previously to membrane permeabilization. However, we were not able to verify the Gm−rhod entry before 2 min probably due to the sensitivity of the fluorescence methodology. The time interval observed until the $[Ca^{2+}]_c$ increase and the activity displayed by D-Gm (cytotoxicity and induction of $[Ca^{2+}]_c$ increase) also suggest that the effects of Gm are mediated by an independent receptor activation pathway. Thus, the main mechanism of Gm entry involves passive diffusion through the cell membrane, although endocytic mechanisms cannot be excluded.

Once Gm has entered the cells, our observations support a direct action of Gm on organelle membranes. Among the

dx.doi.org/10.1021/mp300251j | Mol. Pharmaceutics 2012, 9, 2686−2697

intracellular alterations induced by Gm, those occurring in the ER were first observed. These morphological alterations could be related to the release of Ca^{2+} from the ER, which is the first component in the Ca^{2+} signaling induced by Gm, and to its loss of function (Figure 2B). Therefore, the morphological alterations and the loss of ER function, followed by the release of $[Ca^{2+}]_{ER}$, would open the SOCC, which is associated with the second phase of the $[Ca^{2+}]_c$ response (Figure 3B). Relative to the participation of mitochondria in Gm-induced cell death, the $[Ca^{2+}]_{mit}$ response also exhibited two oscillatory phases. The first oscillatory phase of $[Ca^{2+}]_{mit}$ elevation occurs simultaneously with the initial phase of $[Ca^{2+}]_c$ (Figure 2A), whereas the second $[Ca^{2+}]_{mit}$ oscillatory phase occurs at the same time as the sustained $[Ca^{2+}]_c$ phase (Figure 2A and 4F) and is dependent on external Ca^{2+}. Mitochondria calcium uptake is tightly regulated and occurs at ER−mitochondria contacts, where microdomains of high calcium concentration are present.[28] This event causes a variety of responses depending on the amount of Ca^{2+} increase, from stimulation of metabolism and ATP production to PTP opening and apoptosis.[28,29] In addition, mitochondrial Ca^{2+} uptake is electrophoretic; thus, increasing the $[Ca^{2+}]_c$ decreases the Ψ_{mit}.[30,31] The restoration of the $\Delta\Psi_{mit}$ is usually a transient process; however, the sustained $[Ca^{2+}]_c$ response promotes the accumulation of $[Ca^{2+}]_{mit}$ and increases the ROS levels (Figure 4 and Figure 5C). Mitochondria represent also the privileged site of ROS production. ROS may act as signaling molecules, inducing a prosurvival autophagic response, or may cause damage to cellular components and apoptotic cell death. ROS production is induced by oxidative stress, which activates cellular signaling. Mitochondria are also targets of ROS damage. Gm induces accumulation of $[Ca^{2+}]_{mit}$ and increases the ROS levels, and both these effects can lead to the total loss of Ψ_{mit}. There is evidence that mitochondrial calcium overload leads to cell death.[29,30,32,33]

Some reports have shown that AMPs and cell-penetrating peptides, such as microcin J25 and lactoferricin, target the mitochondria, leading to apoptosis.[22,34] However, AMPs do not necessarily exhibit similar cell death mechanisms. For instance, tachyplesin, which possesses a β-sheet structure similar to Gm, effectively permeabilized both bacterial and artificial lipid membranes;[16] rather apoptosis was induced in human myeloid leukemia (HL60) cells.[16] On the other hand, tachyplesin induced cell death in a prostate cancer cell line by membrane permeabilization.[2] Similar to tachyplesin, Gm demonstrates different modes of action in different models of cell membranes. It has been suggested that Gm may induce cell death by opening pores in cellular membranes or may possess a detergent-like effect that results in membrane permeabilization in pathogens.[11,35−37] In mammalian cells, Gm promoted cell death by membrane permeabilization in melanoma B16 cells,[1] in human neuroblastoma SH-SY5Y and in rat pheochromocytoma PC12 cells.[25] Recently, different cell death modes of β-hairpin AMPs in erythroleukemia K562 cells were demonstrated.[38] Gm simultaneously promotes apoptosis and membrane permeabilization.[38] Moreover, most of the alterations induced in CHO cells by Gm were also demonstrated to occur in B16 melanoma cells, including membrane permeabilization, loss of Ψ_{mit}, Ca^{2+} increase and morphological alterations (Supporting Information, Figure S6). Furthermore, Gm cytotoxicity to different cell types was evaluated and the IC_{50} is shown in the Supporting Information (Table 1S).

In summary (Figure 7), we demonstrate that the rapid membrane permeabilization of CHO cells induced by Gm was preceded by $[Ca^{2+}]_c$ elevation. Moreover, we provide evidence that Gm entered the cells and induced Ca^{2+} release from the ER, thus promoting a great disturbance in organelles prior to membrane permeabilization. The $[Ca^{2+}]_c$ increase was followed by the disruption of mitochondria and lysosomes. We conclude that the trigger of membrane permeabilization is controlled by a Ca^{2+}-dependent mechanism and involves the disruption of organelles, such as the ER, mitochondria and lysosomes, prior to the loss of membrane integrity.

■ ASSOCIATED CONTENT

Supporting Information

Additional information as discussed in the text, in the form of a table, figures, and movies. This material is available free of charge via the Internet at http://pubs.acs.org.

■ AUTHOR INFORMATION

Corresponding Author

*Departamento de Bioquímica, Universidade Federal de São Paulo, R. Três de Maio, 100, 04044-020, São Paulo, SP, Brazil. Tel: +55(11) 5576-4442. Fax: +55(11) 5573-6407. E-mail: G.Z.J., giselle.zenker@unifesp.br; I.L.S.T., ivarne@umc.br.

Author Contributions

§These authors contributed equally to this work

Notes

The authors declare no competing financial interest.

■ ACKNOWLEDGMENTS

This work was supported by (to E.J.P.-G.) from the "Fundação de Amparo à Pesquisa do Estado de São Paulo" (FAPESP; Grant No. 2009/54869-2) and the Conselho Nacional de Desenvolvimento Científico e Tecnológico (CNPq). R.L.C.-R. was supported by a master's fellowship from CAPES. Additional support was from Fundación Teófilo Hernando, Madrid Spain; a grant to M.F.C.-A. from Consolodación de grupos UAM-CAM (Grant No. 1004040047); and Grant No. AP2009-0343 to A.J.M.-O., FPU program from Ministerio de Educación, Spain.

■ REFERENCES

(1) Rodrigues, E. G.; Dobroff, A. S.; Cavarsan, C. F.; Paschoalin, T.; Nimrichter, L.; Mortara, R. A.; Santos, E. L.; Fazio, M. A.; Miranda, A.; Daffre, S.; Travassos, L. R. Effective topical treatment of subcutaneous murine B16F10-Nex2 melanoma by the antimicrobial peptide gomesin. *Neoplasia* **2008**, *10*, 61−68.

(2) Chen, J.; Xu, X. M.; Underhill, C. B.; Yang, S.; Wang, L.; Chen, Y.; Hong, S.; Creswell, K.; Zhang, L. Tachyplesin activates the classic complement pathway to kill tumor cells. *Cancer Res.* **2005**, *65*, 4614−4622.

(3) Hoskin, D. W.; Ramamoorthy, A. Studies on anticancer activities of antimicrobial peptides. *Biochim. Biophys. Acta* **2008**, *1778*, 357−375.

(4) Paredes-Gamero, E. J.; Nogueira-Pedro, A.; Miranda, A.; Justo, G. Z. Hematopoietic modulators as potential agents for the treatment of leukemia. *Front. Biosci.* **2012**, in press.

(5) Silva, P. I., Jr.; Daffre, S.; Bulet, P. Isolation and characterization of gomesin, an 18-residue cysteine-rich defense peptide from the spider Acanthoscurria gomesiana hemocytes with sequence similarities to horseshoe crab antimicrobial peptides of the tachyplesin family. *J. Biol. Chem.* **2000**, *275*, 33464−33470.

(6) Barbosa, F. M.; Daffre, S.; Maldonado, R. A.; Miranda, A.; Nimrichter, L.; Rodrigues, M. L. Gomesin, a peptide produced by the spider Acanthoscurria gomesiana, is a potent anticryptococcal agent that acts in synergism with fluconazole. *FEMS Microbiol. Lett.* **2007**, *274*, 279−286.

(7) Moreira, C. K.; Rodrigues, F. G.; Ghosh, A.; Varotti Fde, P.; Miranda, A.; Daffre, S.; Jacobs-Lorena, M.; Moreira, L. A. Effect of the antimicrobial peptide gomesin against different life stages of Plasmodium spp. *Exp. Parasitol.* **2007**, *116*, 346−353.

(8) Burgierman, M. R. Atividade do peptídeo antimicrobiano gomesina contra *Trypanosoma cruzi* e *Leishmania spp*; Universidade de São Paulo, São Paulo, 2003.
(9) Silva, P. I.; Daffre, S.; Bulet, P. Isolation and characterization of gomesin, an 18-residue cysteine-rich defense peptide from the spider Acanthoscurria gomesiana hemocytes with sequence similarities to horseshoe crab antimicrobial peptides of the tachyplesin family. *J. Biol. Chem.* **2000**, *275*, 33464−33470.
(10) Del Valle, L.; Pina-Oviedo, S. HIV disorders of the brain: pathology and pathogenesis. *Front. Biosci.* **2006**, *11*, 718−732.
(11) Fazio, M. A.; Oliveira, V. X., Jr.; Bulet, P.; Miranda, M. T.; Daffre, S.; Miranda, A. Structure-activity relationship studies of gomesin: importance of the disulfide bridges for conformation, bioactivities, and serum stability. *Biopolymers* **2006**, *84*, 205−218.
(12) Tamba, Y.; Yamazaki, M. Magainin 2-induced pore formation in the lipid membranes depends on its concentration in the membrane interface. *J. Phys. Chem. B* **2009**, *113*, 4846−4852.
(13) Imura, Y.; Nishida, M.; Ogawa, Y.; Takakura, Y.; Matsuzaki, K. Action mechanism of tachyplesin I and effects of PEGylation. *Biochim. Biophys. Acta* **2007**, *1768*, 1160−1169.
(14) Domingues, T. M.; Riske, K. A.; Miranda, A. Revealing the lytic mechanism of the antimicrobial peptide gomesin by observing giant unilamellar vesicles. *Langmuir* **2010**, *26*, 11077−11084.
(15) Cruz-Chamorro, L.; Puertollano, M. A.; Puertollano, E.; de Cienfuegos, G. A.; de Pablo, M. A. In vitro biological activities of magainin alone or in combination with nisin. *Peptides* **2006**, *27*, 1201−1209.
(16) Zhang, H. T.; Wu, J.; Zhang, H. F.; Zhu, Q. F. Efflux of potassium ion is an important reason of HL-60 cells apoptosis induced by tachyplesin. *Acta Pharmacol. Sin.* **2006**, *27*, 1367−1374.
(17) Paredes-Gamero, E. J.; Leon, C. M.; Borojevic, R.; Oshiro, M. E.; Ferreira, A. T. Changes in intracellular Ca2+ levels induced by cytokines and P2 agonists differentially modulate proliferation or commitment with macrophage differentiation in murine hematopoietic cells. *J. Biol. Chem.* **2008**, *283*, 31909−31919.
(18) Barbosa, C. M.; Leon, C. M.; Nogueira-Pedro, A.; Wasinsk, F.; Araujo, R. C.; Miranda, A.; Ferreira, A. T.; Paredes-Gamero, E. J. Differentiation of hematopoietic stem cell and myeloid populations by ATP is modulated by cytokines. *Cell Death Dis.* **2011**, *2*, e165.
(19) Leon, C. M.; Barbosa, C. M.; Justo, G. Z.; Borelli, P.; Resende, J. D., Jr.; de Oliveira, J. S.; Ferreira, A. T.; Paredes-Gamero, E. J. Requirement for PLCgamma2 in IL-3 and GM-CSF-stimulated MEK/ERK phosphorylation in murine and human hematopoietic stem/progenitor cells. *J. Cell Physiol.* **2011**, *226*, 1780−1792.
(20) Bose, D. D.; Rahimian, R.; Thomas, D. W. Activation of ryanodine receptors induces calcium influx in a neuroblastoma cell line lacking calcium influx factor activity. *Biochem. J.* **2005**, *386*, 291−296.
(21) Iredale, P. A.; Hill, S. J. Increases in intracellular calcium via activation of an endogenous P2-purinoceptor in cultured CHO-K1 cells. *Br. J. Pharmacol.* **1993**, *110*, 1305−1310.
(22) Niklison-Chirou, M. V.; Dupuy, F.; Pena, L. B.; Gallego, S. M.; Barreiro-Arcos, M. L.; Avila, C.; Torres-Bugeau, C.; Arcuri, B. E.; Bellomio, A.; Minahk, C.; Morero, R. D. Microcin J25 triggers cytochrome c release through irreversible damage of mitochondrial proteins and lipids. *Int. J. Biochem. Cell Biol.* **2010**, *42*, 273−281.
(23) Filippin, L.; Magalhaes, P. J.; Di Benedetto, G.; Colella, M.; Pozzan, T. Stable interactions between mitochondria and endoplasmic reticulum allow rapid accumulation of calcium in a subpopulation of mitochondria. *J. Biol. Chem.* **2003**, *278*, 39224−39234.
(24) Filippin, L.; Abad, M. C.; Gastaldello, S.; Magalhaes, P. J.; Sandona, D.; Pozzan, T. Improved strategies for the delivery of GFP-based Ca2+ sensors into the mitochondrial matrix. *Cell Calcium* **2005**, *37*, 129−136.
(25) Soletti, R. C.; del Barrio, L.; Daffre, S.; Miranda, A.; Borges, H. L.; Moura-Neto, V.; Lopez, M. G.; Gabilan, N. H. Peptide gomesin triggers cell death through L-type channel calcium influx, MAPK/ERK, PKC and PI3K signaling and generation of reactive oxygen species. *Chem.-Biol. Interact.* **2010**, *186*, 135−143.
(26) Takeshima, K.; Chikushi, A.; Lee, K. K.; Yonehara, S.; Matsuzaki, K. Translocation of analogues of the antimicrobial peptides magainin and buforin across human cell membranes. *J. Biol. Chem.* **2003**, *278*, 1310−1315.
(27) Sonawane, A.; Santos, J. C.; Mishra, B. B.; Jena, P.; Progida, C.; Sorensen, O. E.; Gallo, R.; Appelberg, R.; Griffiths, G. Cathelicidin is involved in the intracellular killing of mycobacteria in macrophages. *Cell Microbiol.* **2011**, *13*, 1601−1617.
(28) Rizzuto, R.; Brini, M.; Murgia, M.; Pozzan, T. Microdomains with high Ca2+ close to IP3-sensitive channels that are sensed by neighboring mitochondria. *Science* **1993**, *262*, 744−747.
(29) Mammucari, C.; Rizzuto, R. Signaling pathways in mitochondrial dysfunction and aging. *Mech. Ageing Dev.* **2010**, *131*, 536−543.
(30) Jacobson, J.; Duchen, M. R. Mitochondrial oxidative stress and cell death in astrocytes–requirement for stored Ca2+ and sustained opening of the permeability transition pore. *J. Cell Sci.* **2002**, *115*, 1175−1188.
(31) Duchen, M. R. Mitochondria and Ca(2+)in cell physiology and pathophysiology. *Cell Calcium* **2000**, *28*, 339−348.
(32) Kuznetsov, A. V.; Margreiter, R.; Amberger, A.; Saks, V.; Grimm, M. Changes in mitochondrial redox state, membrane potential and calcium precede mitochondrial dysfunction in doxorubicin-induced cell death. *Biochim. Biophys. Acta* **2011**, *1813*, 1144−1152.
(33) Liang, H. L.; Sedlic, F.; Bosnjak, Z.; Nilakantan, V. SOD1 and MitoTEMPO partially prevent mitochondrial permeability transition pore opening, necrosis, and mitochondrial apoptosis after ATP depletion recovery. *Free Radical Biol. Med.* **2010**, *49*, 1550−1560.
(34) Mader, J. S.; Richardson, A.; Salsman, J.; Top, D.; de Antueno, R.; Duncan, R.; Hoskin, D. W. Bovine lactoferricin causes apoptosis in Jurkat T-leukemia cells by sequential permeabilization of the cell membrane and targeting of mitochondria. *Exp. Cell Res.* **2007**, *313*, 2634−2650.
(35) Moraes, L. G.; Fazio, M. A.; Vieira, R. F.; Nakaie, C. R.; Miranda, M. T.; Schreier, S.; Daffre, S.; Miranda, A. Conformational and functional studies of gomesin analogues by CD, EPR and fluorescence spectroscopies. *Biochim. Biophys. Acta* **2007**, *1768*, 52−58.
(36) Schaeffer, M.; de Miranda, A.; Mottram, J. C.; Coombs, G. H. Differentiation of Leishmania major is impaired by over-expression of pyroglutamyl peptidase I. *Mol. Biochem. Parasitol.* **2006**, *150*, 318−329.
(37) Moreira, C. K.; Rodrigues, F. G.; Ghosh, A.; Varotti Fde, P.; Miranda, A.; Daffre, S.; Jacobs-Lorena, M.; Moreira, L. A. Effect of the antimicrobial peptide gomesin against different life stages of Plasmodium spp. *Exp. Parasitol.* **2007**, *116*, 346−353.
(38) Paredes-Gamero, E. J.; Martins, M. N. C.; Cappabianco, F. A. M.; Ide, J. S.; Miranda, A. Characterization of dual effects induced by antimicrobial peptides: regulated cell death or membrane disruption. *Biochim. Biophys. Acta* **2012**, *1820*, 1062−1072.